# Dynamic axial crushing of aluminium alloy 6063 -T6 circular tubes

## S. S. Hsu and N. Jones*

Impact Research Centre, Department of Engineering
The University of Liverpool
Brownlow Hill, Liverpool L69 3GH

### Abstract

An experimental investigation was carried out to study the behaviour of circular thin-walled aluminium alloy 6063T6 extrusions subjected to large axial impact loadings. The specimens, having an external diameter of 51 mm, were 1.5 mm thick, giving a 2R/H ratio of 33, approximately. Eighteen quasi-static and thirty-seven dynamic tests were performed and the primary variables were the specimen length ($250 \leq L \leq 1200$ mm), the impact mass ($72 \leq G \leq 248$ kg) and the initial velocity ($3.33 \times 10^{-5} \leq V_i \leq 8.33$ m/s) of the impact mass. The two latter variables were combined to give a constant input energy of 2.5 kJ in order to investigate the effect of inertia on the axial crushing of the aluminium alloy tubes without the contributory effect of material strain rate sensitivity.

The tensile stress-strain relations for the aluminium alloy 6063T6 of thickness 1.50 mm have been experimentally determined at room temperature (approximately $20^0$C) over a range of overall strain rates from $5 \times 10^{-4}\text{s}^{-1}$ to $118\text{s}^{-1}$, approximately. The yield and the ultimate tensile stresses of the material show a negligible dependency on strain rates, while the overall elongation exhibits a slight minimum at $0.03\text{s}^{-1}$, approximately. The corresponding large values of the Cowper-Symonds coefficients obtained using a least mean square fit, confirmed the strain rate insensitivity of the material.

Keywords: dynamic crushing, circular tubes, aluminium alloy 6063 T6, experiments, global bending, counterintuitive response

### Notation

$\dot{\varepsilon}$ – overall strain rate, total $\varepsilon$ divided by event time
$\dot{\varepsilon}_y$ – strain rate at $\sigma_{0.2}$ divided by time to reach 0.2% yield stress
$\dot{\varepsilon}_u$ – strain rate of UTS $\sigma_{0u}$, divided by time to reach UTS
$\sigma$ – engineering stress
$\rho$ – Density
$\delta$ – crushed length
After gl – gauge length after tensile test
D, q – Cowper-Symonds coefficients

T – input energy
$E_h$ – hardening modulus
elongation – (gl-after gl)/gl
G – mass of striker
gl – initial gauge length, 60mm
H – thickness
L – length of specimen
$P_m$ – mean load
$P_p$ – peak load
R – mean radius of tube
UTS – Ultimate Tensile Stress
$V_i$ – impact velocity
W – width of tensile specimen

## 1   Introduction

The mechanics of dynamic plastic deformation of many ductile structures are influenced largely by two factors: the yield or flow stress of the material, which is dependent on the strain rate, and the deformation mode of the structure under dynamic loading which is different to the quasi-static mode on account of inertia forces [5]. The significance of these two factors, either acting separately or together, differs with different types and sizes of structures. For example, the deformation mode of an axially loaded tube might change when the initial tube length is increased or decreased with all of the remaining parameters unchanged. This transition length can be influenced by inertia forces.

Previous experimental studies on this phenomenon have examined the axial impact behaviour of mild steel [1], aluminium alloy [8] and stainless steel [7] tubes and a comparison between the behaviour of these three different materials has been made in Reference [9]. A counterintuitive behaviour has been observed in several experimental [8] and numerical [2, 10, 15, 16] studies and this phenomenon is explored further in the current study for aluminium alloy 6063T6 circular tubes impacted axially.

In the present study, strain rate insensitive aluminium-magnesium-silicon alloy (Al-Mg-Si), grade 6063T6 circular tubes were crushed axially both quasi-statically and dynamically at a standard input energy of 2.5 kJ. The specimens, having an external diameter of 51 mm, were 1.5 mm thick, giving a 2R/H ratio of 33, approximately. This series of tests serves to (a) generate experimental data for the validation of numerical simulations; (b) study the effect of specimen length and inertia on the dynamic behaviour of Al-Mg-Si aluminium shells with a T6 temper, and (c) establish a transitional line separating the regions for progressive collapse and global buckling.

## 2 Material properties

The tube specimens were supplied in two batches, the first consisting of five tubes of 5 m lengths and the second of six tubes having 4 m lengths, from which the tensile specimens were machined. The nominal properties and chemical compositions of this alloy are shown in Table 1 [21]. The room temperature tensile properties of the material were determined from standard quasi-static and dynamic tensile tests. The variations in the thicknesses for the extruded components were between 1.48 mm and 1.55 mm (thickness = 1.518 mm$\pm$ 2.3 per cent, approximately), which is significant and may be an important factor to assess in any numerical modelling.

| Aluminium Alloy | 6063T6 |
|---|---|
| $\rho$, g/cm$^3$ | 2.7 |
| $\sigma_{UTS}$, MPa | 240 |
| $\sigma_Y$, MPa | 215 |
| Elongation % (in 50mm) | 12 |
| E, Gpa | 69 |
| Al, Wt % | 98.9 |
| Cr | Max 0.1 |
| Cu | Max 0.1 |
| Fe | Max 0.35 |
| Mg | 0.45 − 0.9 |
| Mn | Max 0.1 |
| Si | 0.2 − 0.6 |
| Ti | Max 0.1 |
| Zn | Max 0.1 |

Table 1: Material properties and composition of aluminium alloy 6063T6 [21].

### 2.1 Tensile tests

The tubes were cut in half across the cross-section and rolled flat. Tensile test specimens were then cut along the longitudinal direction of the tubing as 30 mm wide strips by 300 mm long.

The standard procedure for quasi-static tensile testing was conducted on an INSTRON 4204 tensile test machine. The head speed was set to 2mm/min giving an average overall strain rate, $\dot{\varepsilon}_u$, of 5 x $10^{-4}$s$^{-1}$, approximately, for a gauge length of 60mm. The dynamic tensile tests were undertaken on a high-speed displacement controlled electro-servo hydraulic (ESH) machine at strain rates from $2 \times 10^{-2}$ to 118s$^{-1}$. All the test specimens, except for two that were loaded quasi-statically, were strain gauged symmetrically on the front and back sides of the head and body. At least two specimens were examined at each test speed. The tensile tests results are

outlined in Table 2. The quasi-static 0.2% yield stress and UTS are 225MPa and 268MPa, respectively, and the rupture strain for a gauge length of 60mm is 8.9%. Figure 1 shows selected engineering stress-strain curves for the specimens at each test speed.

| Specimen | W (mm) | H (mm) | gl (mm) | after gl (mm) | Overall Elongation (strain) | Test Speed (mm/s) | Event time (s) | $\dot{\varepsilon}_y$ | $\dot{\varepsilon}_u$ | $\sigma_U$ (MPa) | $\sigma_y$ 0.1% | 0.2% | $E_h^*$ (MPa) | $\dot{\varepsilon}$ |
|---|---|---|---|---|---|---|---|---|---|---|---|---|---|---|
| AA2 | 9.99 | 1.48 | 59.96 | 65.84 | 0.098 | 0.0333 | 195 | 0.000556 | | 271 | 220 | 227 | 300 | 0.000503 |
| AA3 | 9.98 | 1.51 | 59.96 | 65.26 | 0.088 | 0.0333 | 176 | 0.000556 | | 271 | 220 | 227 | 300 | 0.000502 |
| AA20 | 10.02 | 1.53 | 60.67 | 65.56 | 0.081 | 0.0333 | 150 | 0.000549 | | 261 | 207 | 222 | 300 | 0.000537 |
| AA1 | 10.01 | 1.53 | 60.15 | 65.05 | 0.081 | 2.000 | | | | | | | | |
| AA8 | 10.01 | 1.55 | 60.82 | 65.14 | 0.071 | 2.161 | 2.917 | 0.0029 | 0.0236 | 273 | 224 | 237 | 300 | 0.0244 |
| AA13 | 9.97 | 1.48 | 59.30 | 64.54 | 0.088 | 2.0476 | 2.897 | 0.0029 | | 275 | 223 | 231 | 300 | 0.0305 |
| AA9 | 10.02 | 1.51 | 60.19 | 65.29 | 0.085 | 14.866 | 0.3288 | 0.0250 | 0.1804 | 268 | 217 | 232 | 300 | 0.2577 |
| AA4 | 10.00 | 1.52 | 59.29 | 64.31 | 0.085 | 14.065 | 0.4468 | 0.0320 | 0.1771 | 278 | 219 | 237 | 300 | 0.1895 |
| AA19 | 10.00 | 1.52 | 59.04 | 64.08 | 0.085 | 12.299 | 0.4950 | 0.0375 | 0.124 | 269 | 219 | 231 | 300 | 0.1725 |
| AA17 | 10.00 | 1.52 | 59.96 | 65.09 | 0.086 | 164.2 | 0.0434 | 0.1772 | 1.7697 | 272 | 218 | 233 | 300 | 1.970 |
| AA7 | 10.02 | 1.52 | 60.26 | 65.52 | 0.087 | 160.11 | 0.0462 | 0.24 | 2.0072 | 274 | 223 | 237 | 300 | 1.888 |
| AA6 | 9.97 | 1.55 | 59.29 | 64.62 | 0.090 | 146.62 | 0.0500 | 0.17 | 1.2438 | 277 | 221 | 238 | 300 | 1.798 |
| AA16 | 9.99 | 1.50 | 59.33 | 64.37 | 0.085 | 1502 | 0.0073 | 8.39 | 10.463 | 268 | 224 | 240 | 300 | 11.589 |
| AA12 | 10.04 | 1.51 | 59.81 | 65.43 | 0.094 | 1500 | | | | | | | | |
| AA11 | 10.02 | 1.52 | 59.45 | 64.73 | 0.089 | 1338 | 0.0057 | 4.63 | 15.00 | 277 | 216 | 250 | 300 | 15.609 |
| AA14 | 10.02 | 1.53 | 60.05 | 65.70 | 0.094 | 1434 | 0.0054 | 5.19 | 15.72 | 270 | 216 | 236 | 300 | 17.347 |
| AA15 | 10.04 | 1.53 | 59.16 | 65.36 | 0.105 | 7179 | 0.0009 | 44.08 | 77.93 | 282 | 226 | 230 | 300 | 117.8 |
| AA18 | 10.02 | 1.52 | 59.34 | 64.37 | 0.085 | 7341 | 0.0008 | 44.67 | 79.48 | 278 | 231 | 242 | 300 | 107.6 |

* slope of engineering stress-strain curve at 2% strain, approximately

Table 2: Tensile test results.

The behaviour of the 0.2% proof stress and UTS with respect to their respective strain rates are shown in Figures 2 and 3. As anticipated, this grade of aluminium alloy is virtually strain rate insensitive, which is consistent with many studies published previously [4, 6, 14, 22, 24]. Nonetheless an initial inspection of Figures 2 and 3 does reveal a slight increase in the 0.2% yield stress and UTS over the associated quasi-static values. A similar behaviour is observed for the proof stresses at strains of 1%, 2% and 5%. The corresponding increases in the flow stress at 0.2% proof stress and the UTS ($\varepsilon > 0.05$) are both 5% when the overall strain rate was increased from 0.0005 to $118s^{-1}$. This behaviour may be compared with an increase of 12% in the UTS reported by Nicholas [22] for a similar grade of aluminium alloy, 6061T6, for strain rates up to 600 $s^{-1}$. He revealed a negligible increase in the stress-strain curves up to approximately 10 $s^{-1}$ after which a greater degree of rate sensitivity at higher strain rates prevailed. Steidel and Makerov [14] found the UTS increased 5% for strain rates up to $69s^{-1}$, also for type 6061T6. It was concluded by Davies and Magee [6] that aluminium alloy 6061T6 had low a rate dependency for strain rates up to $830s^{-1}$.

The overall elongations of the specimens were between 7.1% and 10.5% for a gauge length of 60mm, as shown in Figure 4 as a function of the overall strain rate. In spite of the experimental scatter, the average elongation appears to decrease to a minimum at $0.03s^{-1}$ and increases gradually to beyond the quasi-static values at $118s^{-1}$. This phenomenon has been observed to be more pronounced and distinct for stainless steel [7].
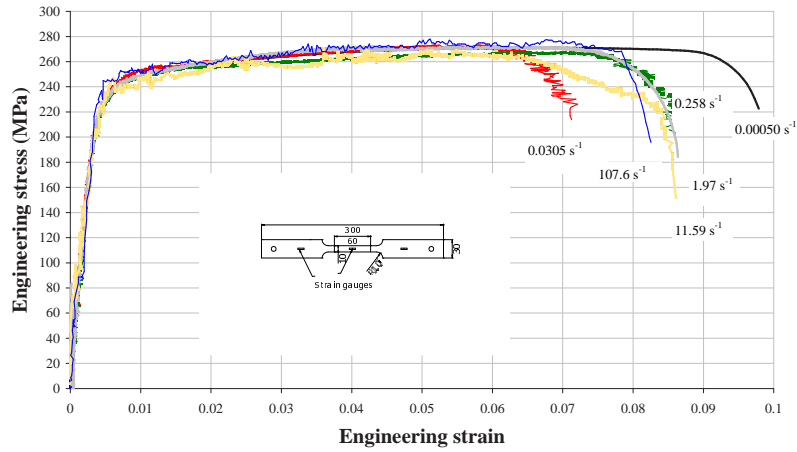
Figure 1: Engineering stress-strain curve at six different strain rates.
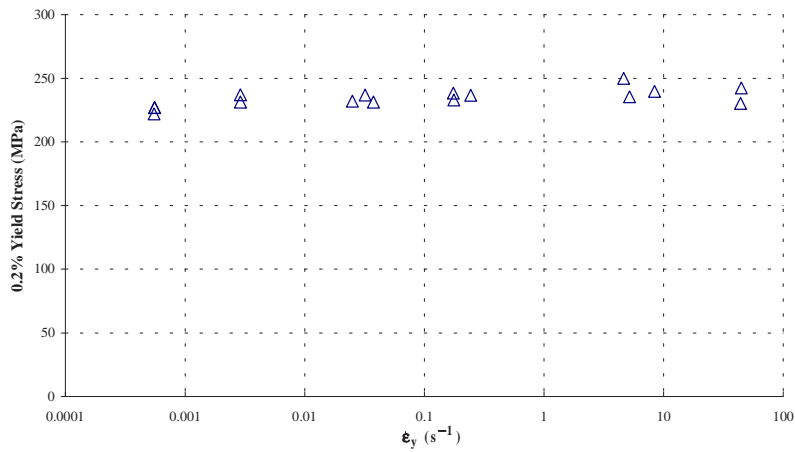


Figure 2: Variation of the 0.2% proof stress with strain rate.
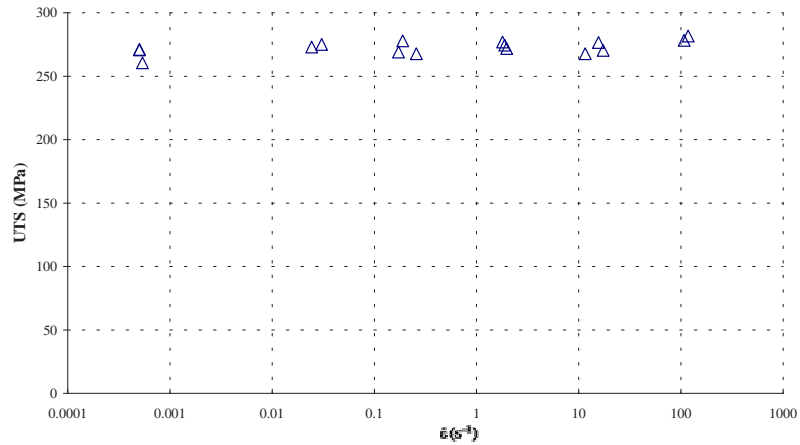
Figure 3: Variation of the UTS with strain rate.
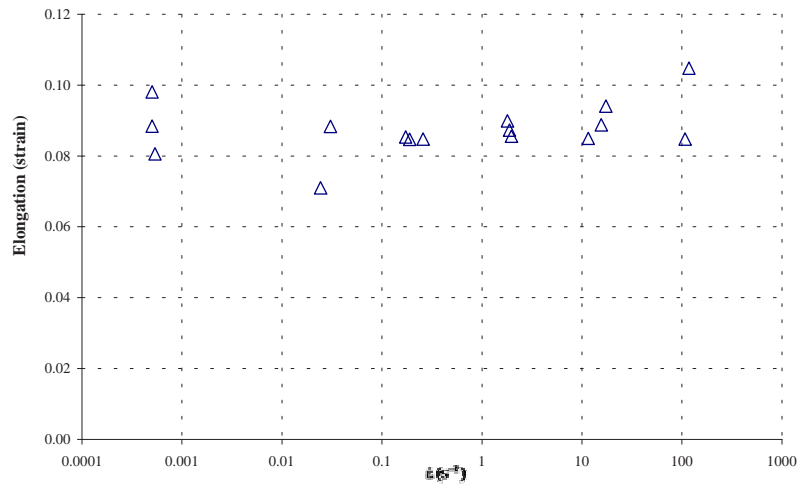


Figure 4: Variation of the total elongation with strain rate.

The data in Figures 2 and 3 are re-plotted in Figures 5 and 6, respectively, which give the Cowper-Symonds coefficients [13] at the two flow stresses using a least mean square fit. At yield, $D = 9.390 \times 10^{10} s^{-1}$ and $q = 9.55$ and at the UTS, $D = 4.7076 \times 10^{13}$ $s^{-1}$ and $q = 10.16$. These values are much higher than the values of $D = 6500 s^{-1}$ and $q = 4$ which are listed in Reference [13] and noted in Reference [4]. An earlier study [12] into the strain rate sensitive behaviour of aluminium alloy 6061T6 observed that the Cowper-Symonds equation with $D = 1.288 \times 10^6 s^{-1}$ and $q = 4$ passed through the average of the widely scattered data of several experimental programs. The high values of D confirm the negligible strain rate sensitivity of

this material.

It should be noted that the average Vicker's hardness number of the axially crushed tubes is 78.3, while that for tensile test specimens is 97.5. The larger hardness numbers for the tensile test specimens is presumably due to the flattening process, which may have changed the mechanical properties of the aluminium alloy. If it is assumed that the Vicker's hardness number has a linear relationship with the UTS (a linear relationship with the Brinell hardness number has been used in Reference [23]), then the UTS of an untested tube, which has an average Vicker's hardness number of 80.6, would be $2.814^1 \times 80.6 = 226.8$MPa. This is about 15% smaller than the average UTS of 268MPa recorded in the tensile tests. Therefore, it raises questions on the accuracy of any numerical simulations which use constitutive relationships based on tensile specimens cut from flattened circular tubes.

## 3   Axial crushing of tubes

Eighteen quasi-static and thirty-seven dynamic tests were performed in the current study. Details of the tube lengths, impact masses and the corresponding impact velocities, which are calculated when assuming that a drop was frictionless, are listed in Table 3, while the quasi-static results are included in Table 2 of Reference [9]. The mean load, $P_m$, is defined as the total input energy, i.e. the initial kinetic energy, divided by the permanent axial crushing distance of a specimen, and was only calculated for specimens that collapse progressively. An input energy of 2.5KJ was adopted as a standard for all the dynamic tests in Table 3 and was chosen since it produced a reasonable number of complete wrinkles ($\approx 6$) in a circular tube. The energy of 2.5KJ was imparted by dropping one of six different tup masses from the appropriate height.

Table 3: Summary of dynamic axial crushing tests.

| Test ID | L (mm) | $\delta$ (mm) | G (kg) | $V_i$ (m/s) | $P_m$ (kN) | Failure Mode |
|---------|--------|---------------|--------|-------------|------------|--------------|
| DAASC42 | 700 | 68 | 72 | 8.33 | 36.8 | A(5) bottom, slight bending 1/3 top |
| DAASC43 | 850 | 87 | 72 | 8.33 | 28.7 | A(2) top, A(4) bottom, sequence unknown, slight bending 1/3 top with slight wrinkles |
| DAASC44 | 1005 | | 72 | 8.33 | | no wrinkles on first impact, OB on secondary impact, bending wrinkles at 1/3 bottom |
| DAASC45 | 1200 | | 72 | 8.33 | | bending wrinkles along top 1/3, top 1/4 broke off |

[1]2.814 is the average of all UTS values divided by the corresponding Vicker's hardness value from the tensile test.

Table 3: Summary of dynamic axial crushing tests.

| | | | | | | |
|---|---|---|---|---|---|---|
| DAASC46 | 940 | | 72 | 8.33 | | 2 hinges, 1/3 top and 1/3 bottom |
| DAASC47 | 750 | | 72 | 8.33 | | OB 1/3 top but bending wrinkles at 1/3 bottom |
| DAASC16 | 900 | | 102 | 7.00 | | A(5) bottom, OB 1/3 top, slight bending wrinkles |
| DAASC17 | 1000 | | 102 | 7.00 | | A(1) top, OB above middle and 1/3 top, slight tearing at wrinkle |
| DAASC18 | 800 | | 102 | 7.00 | | A(1) top, OB 1/3 top |
| DAASC19 | 750 | | 102 | 7.00 | | OB 1/3 top, severe tearing at hinge line |
| DAASC20 | 600 | | 102 | 7.00 | | A(4.5) top, OB near top |
| DAASC36 | 450 | 70 | 103 | 6.97 | 35.7 | A(5) top |
| DAASC37 | 500 | | 103 | 6.97 | | OB above middle |
| DAASC38 | 550 | 80 | 103 | 6.97 | 31.3 | A(4) top A(1.5) bottom, slight bending at middle, sequence unknown |
| DAASC39 | 580 | | 103 | 6.97 | | OB above middle |
| DAASC40 | 400 | | 103 | 6.97 | | A(1.5) top, OB above middle |
| DAASC41 | 350 | 94 | 103 | 6.97 | 26.6 | A(7) top |
| DAASC55 | 400 | 83 | 117 | 6.54 | 30.1 | A(2) D(2) top |
| DAASC56 | 500 | | 117 | 6.54 | | A(4.5) top, OB middle |
| DAASC57 | 450 | 82 | 117 | 6.54 | 30.5 | A(5.5) top, slight bending wrinkles at middle |
| DAASC58 | 550 | | 117 | 6.54 | | OB above middle, severe tearing at hinge line |
| DAASC59 | 600 | | 117 | 6.54 | | OB above middle |
| DAASC31 | 650 | | 150 | 5.77 | | OB below middle, severe tearing at hinge line, 2nd hinge at 3 inches from bottom |
| DAASC32 | 600 | | 150 | 5.77 | | OB middle, middle almost severed, 2nd hinge at 3 inches from bottom, slight DPV at bottom |
| DAASC33 | 450 | | 150 | 5.77 | | OB below middle |
| DAASC34 | 350 | 96 | 150 | 5.77 | 26.0 | A(7) top, slight wrinkle at bottom |
| DAASC35 | 400 | | 150 | 5.77 | | OB 1/3 top, severe tearijng at hinge line and all tube due to secondary impact* |
| DAASC60 | 500 | 79 | 149 | 5.79 | 31.6 | A(6) top |

Table 3: Summary of dynamic axial crushing tests.

| DAASC61 | 550 | 78 | 149 | 5.79 | 32.1 | A(5.5) bottom, very slight bending wrinkles at 1/3 top |
|---------|-----|-----|-----|------|------|---|
| DAASC25 | 491 | 85 | 193 | 5.09 | 29.4 | A(3) top A(1) D(1) bottom, tearing at diamond wrinkle, slight bending wrinkles at middle and top |
| DAASC26 | 600 | | 193 | 5.09 | | OB at 1/3 top , severe crumble and tearing at hinge |
| DAASC27 | 550 | 84 | 193 | 5.09 | 29.8 | A(2) D(1) top, tearing at diamond wrinkle, slight bending wrinkles |
| DAASC28 | 650 | | 193 | 5.09 | | OB above middle, slight bending wrinkles near bottom |
| DAASC21 | 550 | 101 | 248 | 4.49 | 24.8 | A(7) bottom |
| DAASC22 | 600 | | 248 | 4.49 | | OB 1/3 top, tearing at hinge line |
| DAASC23 | 650 | | 248 | 4.49 | | OB 1/3 top |
| DAASC24 | 500 | 100 | 248 | 4.49 | 25.0 | A(7) top |

Small font size refers to specimens machined from the first batch of tubes, as with the quasi-statically tested specimens

*secondary impact refers to the rebound of the tup mass

### 3.1 Experimental arrangement

The test arrangement which was employed in previous studies (eg. Ref. [7]) was used in the current study. Briefly, the quasi-static tests were performed on two compression machines: (a) Denison, with a maximum rating of 500kN for tubes shorter than 600mm long and (b) Dartec, with a maximum load of 250kN and a stroke of 100mm for tubes longer than 600mm. Both machines record the load-displacement histories at a constant pre-selected cross-head speed ranging from 2mm/min to 10mm/min, which was specified according to the specimen length. Each specimen was loaded while placed vertically on an anvil block and a test was halted as soon as it became unstable, or when the specimen was judged to have 'bottomed out'. One tube, SAASC17, was strain gauged at three positions to monitor the local strains near the top, bottom and the middle of the tube.

The impact tests were performed on a drop hammer rig (tup mass, $G < 250$kg, initial velocity, $V_i < 14$ m/s). The specimens were loaded axially by a travelling mass while placed vertically on an anvil block. The velocity-time history was monitored by: (a) a Dantec Laser Doppler Anemometry (LDA) system and (b) a Kodak Ektapro high-speed camera with a film speed of
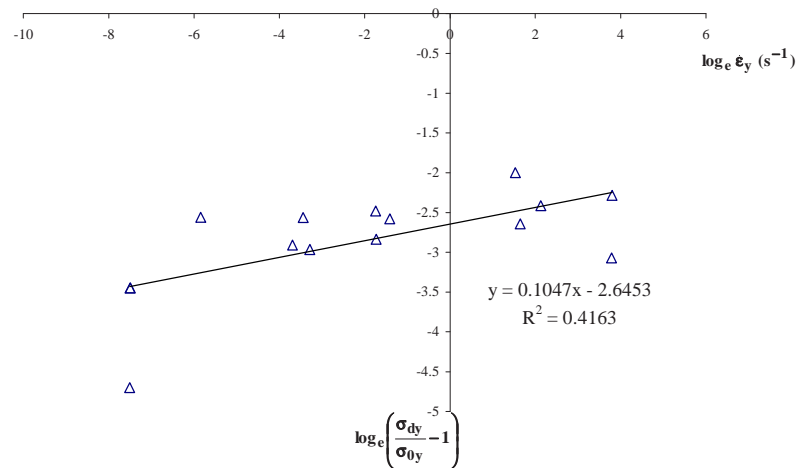
Figure 5: Determination of D and q for the 0.2% proof stress.
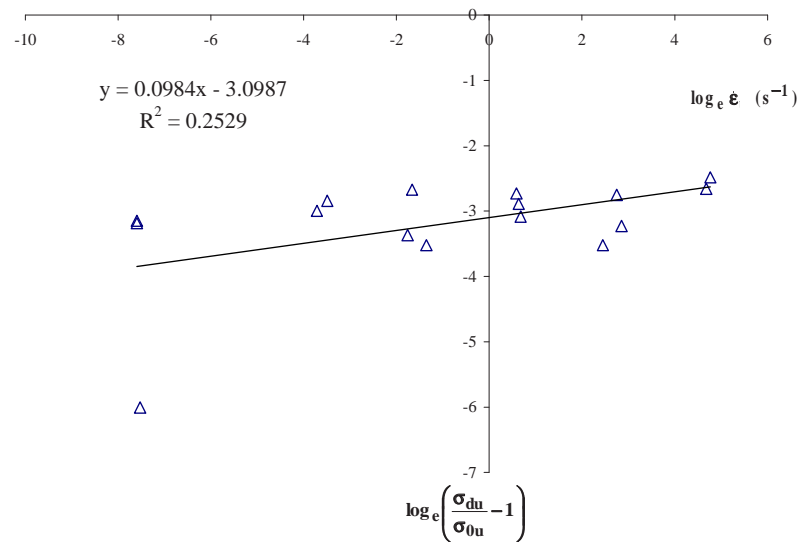


Figure 6: Determination of D and q for the UTS.

2000 frames per second (fps).

## 3.2 Collapse modes

The present tubes exhibit failure modes which are typical for these cross-sections and are similar to those for mild steel [1] and stainless steel [7] tubes. Figure 8 shows photographs of the final shapes of the test specimens for quasi-static (Figure 8(a)) and impact loads (Figure 8(b) - 8(g)) with increasing pre-test lengths from left to right. Three principal modes of failure are identified: axisymmetric (A), also known as concertina, diamond mode (D) and overall bending (OB). The globally bent specimens tended to fail at the middle. Regular progressive collapse, on the other hand, can be initiated at either end with the formation of 7 (or 6 in one case) axisymmetric wrinkles before changing to a diamond mode with three vertices. Internal tearing always occurs on the wrinkle at a transition in a quasi-static test (Figure 9) and was revealed to have taken place on that particular wrinkle during the mode transition by stopping a quasi-static test prematurely. No tearing was observed in any subsequent wrinkles, nor when the tubes deformed only in an axisymetrical mode. The wrinkles initiated more frequently from the proximal end in the dynamic tests (13 out of 14 progressively collapsed tubes), but with no apparent dependence on the magnitude of the impact velocity. Slight internal tearing occurred at the transition wrinkle between axisymmetric and diamond behaviour in only two of the dynamic tests which responded in a progressive buckling mode.

Figure 7 shows three typical quasi-static load-displacement curves of tubes which crushed first in a concertina mode and then switched later to the diamond mode. It is evident that the pattern of behaviour is repeatable. The curves show that the twin peaks merge into a single peak which grows as the number of concertina wrinkles increase until a maximum value is reached, which then decreases immediately before the transition to a diamond mode occurs. The peaks then become smaller and less regular for further deformation.

A 400mm long tube, SAASC17, was strain gauged at 10mm from both ends and in the middle. It is evident from Figure 10(b) that the tube is uniformly compressed axially by 2.5mm, approximately, when the load reaches a peak value and the associated strain readings from the three gauges in Figure 10(a) exceed the plastic limit, i.e., 0.2% proof stress. Thus, the tube is in a state of uniform plastic compression before the development of any local buckling. The maximum recorded strain is 1.9%, approximately, which occurs at the distal end of a quasi-statically loaded tube where a wrinkle is partly (about one-half) formed.

It is noted that the failure modes of progressive collapse and global bending are random within the range $300 \leq L \leq 440$mm for the quasi-static results shown in Figure 8(a). In fact, Jensen et al. [11] observed a similar behaviour for aluminium alloy 6060T6 thin-walled square sections crushed axially. For a given local slenderness ratio, the static behaviour can change from global bending to progressive buckling and back to global bending as the axial length, L, is increased. However, an average value of the critical length for the present tests is 370mm, which turns out to be about 7 per cent larger than 345mm which is estimated from the classification

chart of Andrews et al. [3] for Ht 30 aluminium alloys with $\sigma_{0.1} = 243$ MPa and $\sigma_{0u} = 304$MPa.
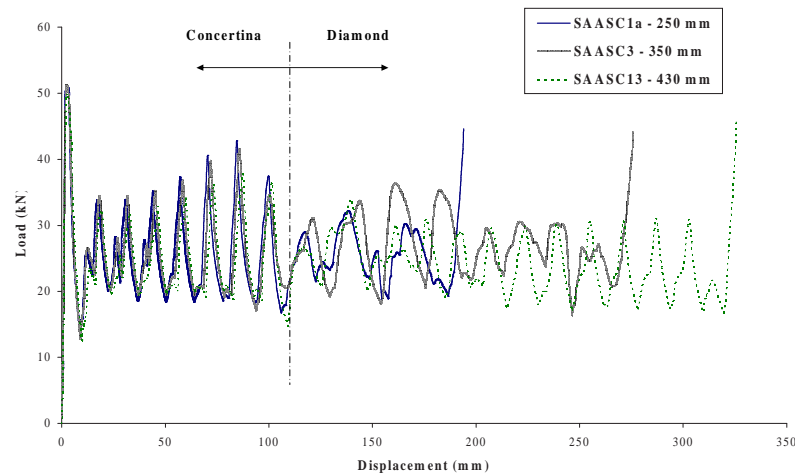


Figure 7: Load-displacement behaviour of three quasi-statically crushed tubes showing a transition between axisymmetric and diamond modes.

## 3.3  Inertia effects

It is well-known that material strain rate sensitivity and inertia effects are dominant features in the dynamic behaviour of Type II structures [5]. By choosing the almost strain rate insensitive aluminium alloy 6063T6 tubes, the effect of strain rate sensitivity can be largely discounted, so that the sole contribution of inertia on the failure mode can be analysed.

The experimental results in Table 3 are plotted in Figure 11 which shows the various failure modes plotted as a function of the initial impact velocity. One feature of this plot is the unexpected scatter of the failure modes for each test mass, which was not noted previously for axial impact tests on stainless steel [7] or mild steel [1] tubes, and which cannot be attributed to experimental error due to the general repeatability of the results.The scatter forms a transitional zone which reveals the sensitivity of the tube behaviour on the specimen length for a given impact velocity.

A transition line was drawn through the experimental data to separate the failure modes into two regions: progressive collapse and overall bending. Clearly, this transition line is different to the curves obtained for similar tests on stainless steel [7] and mild steel [1] tubes. The stability of the tubes increases up to an impact velocity of 5m/s, approximately, and declines for further increases in velocity up to 6.5m/s before improving again. The dip in stability with increase in impact velocity suggests the presence of an 'inverse' response or a counterintuitive phenomenon, as observed by Karagiozova and Alves [17] in the numerical modelling of axially loaded elastic-plastic circular tubes which were made from a strain rate insensitive material. This anomalous

(a) Quasi-static tests: $V_i = 2$ mm/min

(b) G = 72 kg, $V_i$ = 8.33 m/s

(c) G = 102 kg, $V_i$= 7 m/s

(d) G = 117 kg, $V_i$= 6.5 m/s

(e) G = 150 kg, $V_i$ = 5.8 m/s

(f) G = 193 kg, $V_i$ = 5.1 m/s

(g) G = 248 kg, $V_i$ = 4.5 m/s

Figure 8: Final deformation profiles of the test specimens with increasing length from left to right.

Figure 9: Internal tearing of the wrinkle at a transition between axisymmetric (concertina) deformations and the diamond mode for specimen SAASC8 [9].

response has also been observed experimentally for aluminium alloy 6061T6 cylindrical tubes impacted axially in Reference [8] and has been explored numerically in References [10,15,17] and with simple models [16, 18]. The absence of this counterintuitive phenomenon in the dynamic axial crushing of strain-rate sensitive tubes which are made of stainless steel [7] and mild steel [1] suggests that this behaviour may well be a characteristic response of aluminium alloy thin-walled sections which are strain rate insensitive.

The dynamic response of axially impacted tubes consist of two phases of motion; a uniform axial compression which is followed by local bending deformations [15, 16, 19]. Elastic and plastic stress wave propagation play a leading role in the dynamic response during the first phase of motion and the hardening modulus of the material controls the speed of any plastic waves [20]. It was shown in Reference [19] that the inertial resistance due to dynamic loadings having higher impact velocities may cause larger axial strains and stresses to develop during the axial compression phase before the subsequent shell buckling phase. Therefore, less energy is available for any subsequent local bending, which develops at higher stresses due to material strain hardening, thereby causing less deformation for a given amount of absorbed energy. The behaviour in Figure 12 is consistent with this idealisation since the total axial shortening of the specimens ($\delta$) decreases with the impact velocity for a given impact energy. Thus, the mean load increases with the impact velocity (Figure 13) and decreases with the impact mass (Figure 14).

The idealised models in References [16,18], were developed by recognising that a significant amount of impact energy could be absorbed in a wholly axial compression deformation mode before any local wrinkling (dynamic progressive buckling), or global bending, could occur. These idealised models have provided important insight into the complex behaviour of axially impacted elastic-plastic cylindrical shells. Currently, idealised models are being developed to explore the interaction between the different deformation modes rather than studying them largely in isolation as at present.
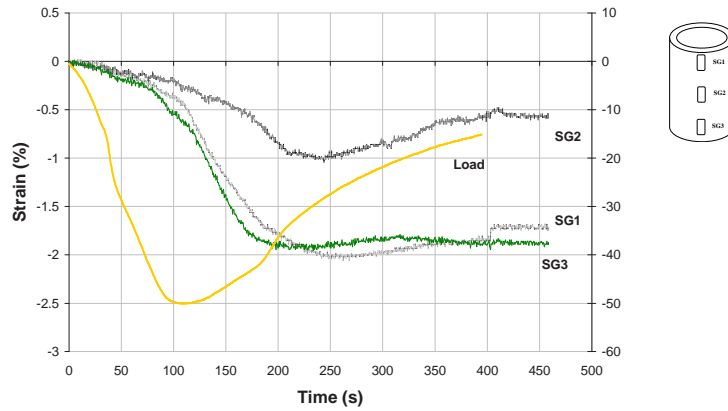
(a) Strain-time and load-time histories of the globally bent specimen SAAC17
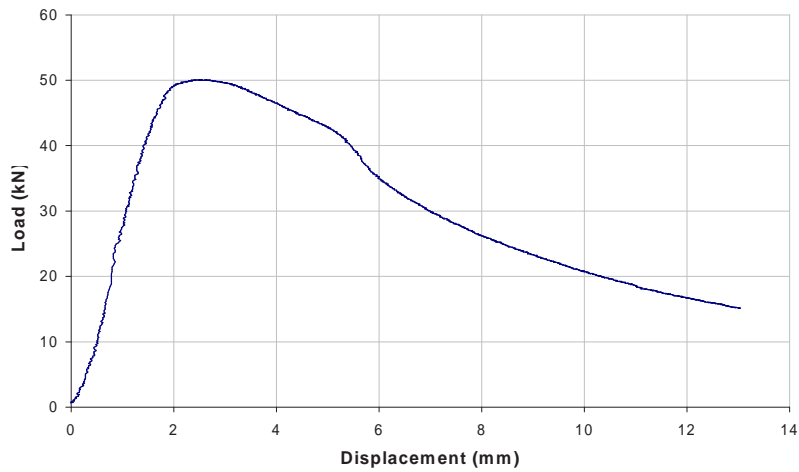


(b) Load- displacement history of specimen SAAC17

Figure 10:
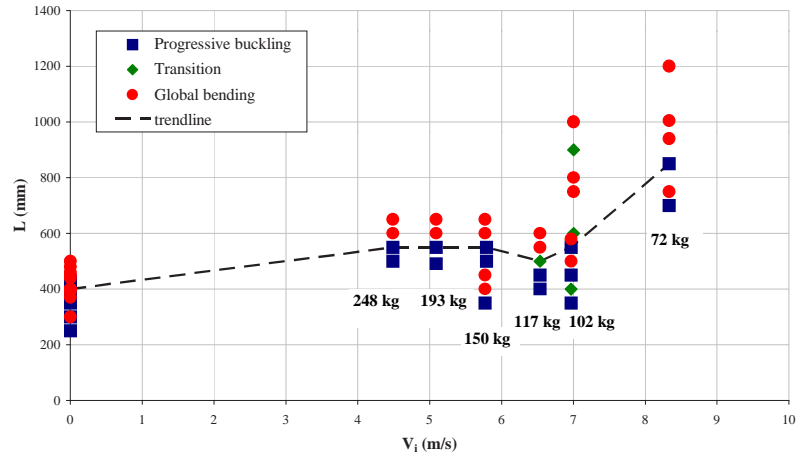
Figure 11: Deformation map for aluminium alloy 6063T6 tubes for an impact energy of 2.5 kJ.
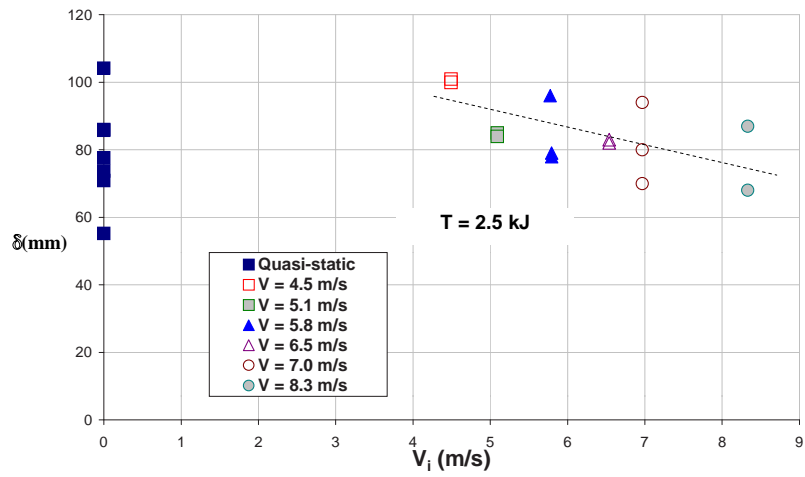


Figure 12: Crushed length against impact velocity.
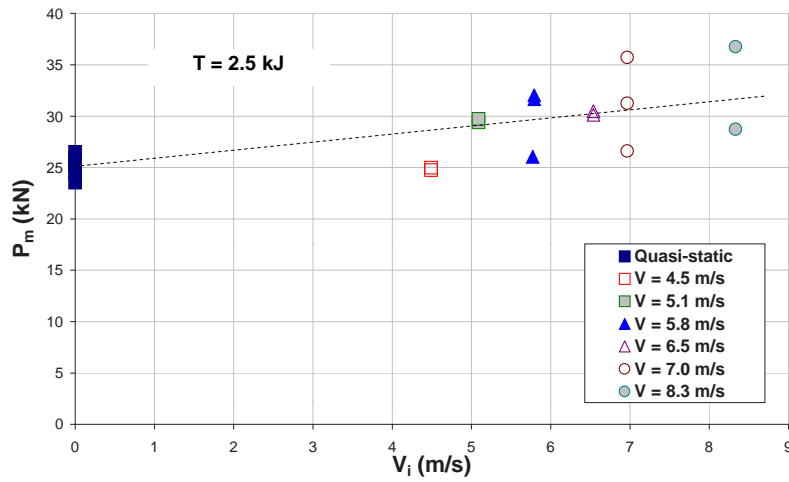
Figure 13: Mean load against impact velocity.
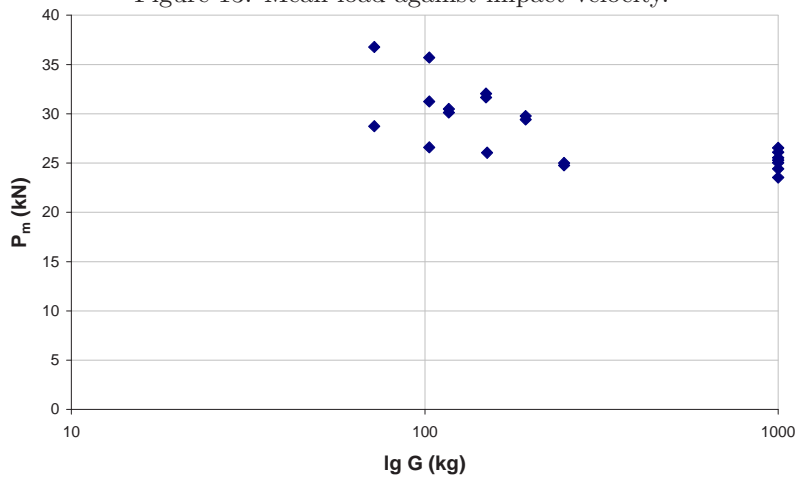


Figure 14: Mean load against impact mass(T=2.5kJ-the impact mass in the quasi-static tests was taken as 1000kg).

## 3.4 Length effect

The total axial shortening of the tubes as a function of the specimen length is plotted in Figure 15 for an impact energy of 2.5kJ. The specimen length does not appear to influence significantly the crushed length for the six impact velocities examined, although there should be a tendency for $\delta$ to decrease as L increases since more energy is absorbed elastically.
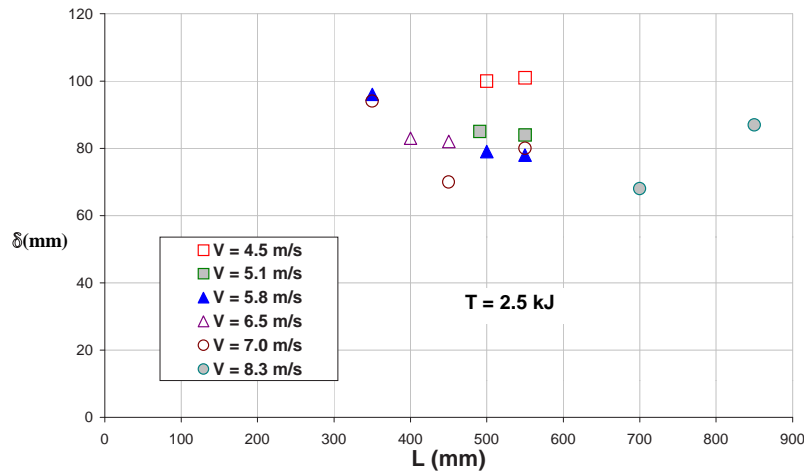
Figure 15: Crushed length against specimen length.

## 4    Conclusions

The material strain rate sensitive characteristics of aluminium alloy 6063T6 have been determined from dynamic tensile tests up to $118$ s$^{-1}$.The results reveal that the yield stress and the UTS of aluminium alloy 6063T6 are essentially rate-insensitive within the investigated range of strain rates, which is consistent with previous results reported in the literature. The elongation, or rupture strain of the material, decreases and then increases with strain rate, showing a slight minimum at $0.03$ s$^{-1}$, approximately.

Experimental results have been reported for the axial compressive behaviour of thin-walled aluminium alloy 6063T6 circular tubes subjected to large axial impact loads. It transpires that the progressive buckling of the aluminium alloy thin walled sections have a tendency towards collapsing in an axisymmetrical mode for the first seven wrinkles before switching to a diamond mode with three-vertices. In the absence of material strain rate effects, it is evident that inertia effects influence the failure modes of the aluminium alloy shells for impact velocities up to 8.33m/s. The experimental results on the aluminium alloy tubes reveal the presence of an 'inverse', or counterintuitive, phenomenon, where the stability of a tube decreases with increase in impact velocity over a small range of velocities rather than continuing to increase. Finally, the initial length of a tube does not appear to have a distinct influence on the crushed length and, thus, the mean load.

## References

[1] W. Abramowicz and N. Jones. Transition from initial global bending to progressive buckling of tubes loaded statically and dynamically. International Journal of Impact Engineering, 19(5/6):415–437, 1997.

[2] M. Alves and D. Karagiozova. Influence of the axial impact velocity on the buckling behaviour of circular cylindrical shells. In proceedings $9^{th}$ National Bulgarian Congress on Theoretical and Applied Mechanics, volume 1, pages pp.388–393, 2001.

[3] K.R.F. Andrews and G.L. England E. Ghani. Classification of the axial collapse of cylindrical tubes under quasi-static loading. International Journal of Mechanical Sciences, 25(9-10):687–696, 1983.

[4] S.R. Bodner and P.S. Symonds. Experimental and theoretical investigation of the plastic deformation of cantilever beams subjected to impulsive loading. Journal of Applied Mechanics, 29:719–728, 1962.

[5] C.R. Calladine and R.W. English. Strain-rate and inertia effects in the collapse of two types of energy-absorbing structure. International Journal of Mechanical Sciences, 26(11/12):689 – 701, 1984.

[6] R. G. Davies and C. L. Magee. The effect of strain-rate upon the tensile deformation of materials. Journal of Engineering Materials and Technology, 97:151–155, 1975.

[7] S.S. Hsu and N. Jones. Quasi-static and dynamic axial crushing of circular and square stainless steel tubes. In N. Jones, C. A. Brebbia, and A. M. Rajendran, editors, Proceedings $7^{th}$ International Conference on Structures Under Shock and Impact, Structures Under Shock and Impact VII, pages 169–178, Southampton and Boston, 2002. WIT Press.

[8] S.S. Hsu and N. Jones. Dynamic axial loading of 6061-T6 aluminium alloy cylindrical shells. In N. K. Gupta, editor, Proceedings $8^{th}$ International Symposium on Plasticity and Impact Mechanics, IMPLAST 2003, pages 411–420, New Delhi, 2003. Phoenix Publishing House.

[9] S.S. Hsu and N. Jones. Quasi-static and dynamic axial crushing of thin-walled circular stainless steel,mild steel and aluminium alloy tubes. International Journal of Crashworthiness, 9(2):195–217, 2004.

[10] O. Jensen, M. Langseth, and O.S. Hopperstad. Transition between progressive and global buckling of aluminium extrusions. In N. Jones, C. A. Brebbia, and A. M. Rajendran, editors, Proceedings of $7^{th}$ International Conference on Structures under Shock and Impact, SUSI VII, pages 269–277, Southampton and Boston, 2002. WIT Press.

[11] O. Jensen, M. Langseth, and O.S. Hopperstad. Transition from local to global buckling: Quasi-static and dynamic experimental results. In N. K. Gupta, editor, Proceedings $8^{th}$ International Symposium on Plasticity and Impact Mechanics, IMPLAST 2003, pages 118–125, New Dehli, 2003. Phoenix Publishing House.

[12] N. Jones. Some remarks on the strain-rate sensitive behaviour of shells. In A. Sawezuk, editor, Problems of Plasticity, volume 2, pages 403–407, Noordhoff, 1974.

[13] N. Jones. Structural Impact. Cambridge University Press, 1997.

[14] R.F. Steidel Jr. and C.E. Makerov. The tensile properties of some engineering materials at moderate rates of strain. ASTM Bulletin, 247:57–64, 1960.

[15] D. Karagiozova. On the dynamic collapse of circular and square tubes under axial impact. In C.A. Brebbia and G.N. Nurick, editors, Advances in Dynamics and Impact Mechanics, pages 1–22, Southampton and Boston, 2003. WIT Press.

[16] D. Karagiozova. Velocity and mass sensitivity of circular and square tubes under axial impact. In N. K. Gupta, editor, proceedings 8th International Symposium on Plasticity and Impact Mechanics, IMPLAST 2003, pages 403–410, New Dehli, 2003. Phoenix Publishing House.

[17] D. Karagiozova and M. Alves. Transition from progressive buckling to global bending collapse of circular shells under axial impact – Part I: Experimental and numerical observations. International Journal of Solids and Structures, 41:1565–1580, 2004.

[18] D. Karagiozova and M. Alves. Transition from progressive buckling to global bending of circular shells under axial impact – Part II: Theoretical analysis. International Journal of Solids and Structures, 41:1581–1604, 2004.

[19] D. Karagiozova, M. Alves, and N. Jones. Inertia effects in axisymmetical deformed cylindrical shells under axial impact. International Journal of Impact Engineering, 24(10):1083–1115, 2000.

[20] D. Karagiozova and N. Jones. Influence of stress waves on the dynamic progressive and dynamic plastic buckling of cylindrical shells. International Journal of Solids and Structures, 38(38/39):6723–6749, 2001.

[21] Matweb. the online materials information resource. http://www.matweb.com/.

[22] T. Nicholas. Tensile testing of materials at high rates of strain. Experimental Mechanics, 21:177–185, 1981.

[23] D. Tabor. The hardness of metals. Oxford University Press, 1951.

[24] P.C. Varley. The technology of aluminium and its alloy. Newnes-Butterworths, London, 1970.